Author(s): Kivisaari, Pyry & Kim, Iurii & Suihkonen, Sami & Oksanen, Jani

Title: Elimination of resistive losses in large-area LEDs by new diffusion-driven devices

Year: 2017

Version: Post print

Please cite the original version:

Kivisaari, Pyry & Kim, Iurii & Suihkonen, Sami & Oksanen, Jani. 2017. Elimination of resistive losses in large-area LEDs by new diffusion-driven devices. Proceedings of SPIE. Volume 10124. 7. DOI: 10.1117/12.2251108.

Elimination of resistive losses in large-area LEDs by new diffusion-driven devices

Pyry Kivisaari[c], Iurii Kim[b], Sami Suihkonen[b], and Jani Oksanen[a]

[a]Engineered Nanosystems Group, Aalto University, P.O. Box 12200, FI-00076 Aalto, Finland
[b]Department of Micro- and Nanosciences, Aalto University, P.O. Box 13000, FI-00076 Aalto, Finland
[c]Division of Solid State Physics and NanoLund, Lund University, P.O. Box 118, SE-22100, Sweden

ABSTRACT

High-power operation of conventional GaN-based light-emitting diodes (LEDs) is severely limited by current crowding, which increases the bias voltage of the LED, concentrates light emission close to the p-type contact edge, and aggravates the efficiency droop. Fabricating LEDs on thick n-GaN substrates alleviates current crowding but requires the use of expensive bulk GaN substrates and fairly large n-contacts, which take away a large part of the active region (AR). In this work, we demonstrate through comparative simulations how the recently introduced diffusion-driven charge transport (DDCT) concept can be used to realize lateral heterojunction (LHJ) structures, which eliminate most of the lateral current crowding. Specifically in this work, we analyze how using a single-side graded AR can both facilitate electron and hole diffusion in DDCT and increase the effective AR thickness. Our simulations show that the increased effective AR thickness allows a substantial reduction in the efficiency droop at large currents, and that unlike conventional 2D LEDs, the LHJ structure shows practically no added efficiency loss or differential resistance due to current crowding. Furthermore, as both electrons and holes enter the AR from the same side without any notable potential barriers in the LHJ structure, the LHJ structure shows an additional wall-plug efficiency gain over the conventional structures under comparison. This injection from the same side is expected to be even more interesting in multiple quantum well structures, where carriers typically need to surpass several potential barriers in conventional LEDs before recombining. In addition to simulations, we also demonstrate selective-area growth of a finger structure suitable for operation as an LHJ device with 2μm distance between n- and p-GaN regions.

—Published in the proceedings of SPIE, Photonics West 2017–

Keywords: Light-emitting diodes, current crowding, diffusion-driven charge transport, selective-area growth, composition grading, high-power operation

1. INTRODUCTION

Highly efficient blue GaN-based light-emitting diodes (LEDs) have disrupted the general lighting industry and are already enabling significant energy savings.[1] However, there are still several issues related to GaN LEDs which, if solved, would provide a higher efficiency at large currents and potentially even new application areas for LEDs[2] and high power visible lasers. One of the present challenges for LED development is current crowding, which typically causes most of the light emission to originate from the p-type contact edge.[3–5] This limits strongly the LED efficiency at current densities above 100 A/cm^2 and therefore prevents LEDs from being used efficiently in applications requiring very high output powers. Very recently, Hurni *et al.* demonstrated how current crowding can be reduced by using a thick n-type current-spreading layer,[6] but this still requires expensive bulk GaN substrates as well as large n-type contacts.

Current transport in today's LEDs is organized using the double heterojunction (DHJ) scheme and the flip-chip design[7] illustrated in Fig. 1(a). The DHJ scheme requires the active region (AR) to be placed between

Send correspondence to pyry.kivisaari@ftf.lth.se

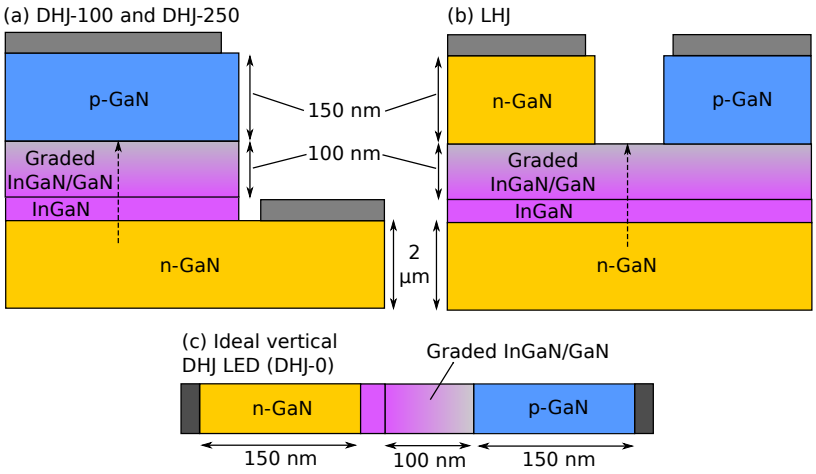

Figure 1. Devices simulated in this work: (a) DHJ-100 and DHJ-250, (b) LHJ and (c) Ideal vertical DHJ LED (DHJ-0). In (a) and (b), the dashed arrows depict where the band diagrams are plotted later in the article. The slight n-type polarization doping in the graded layer is assumed to be compensated with an equal but opposing acceptor doping density.

n- and p-type bulk layers, and this severely limits spreading carriers efficiently over a large-area LED without using a dense n-contact grid that decreases the AR area. In addition, to also keep the additional voltage losses at the contacts at a reasonable level, the n-contact typically has to occupy roughly 10 % of the whole device area, reducing the AR area by an equivalent amount. To provide alternative ways to realize current spreading in optoelectronic devices, we have recently demonstrated the diffusion-driven current transport (DDCT) scheme using simulations and experiments.[8–10] More recently we also proposed that combining DDCT with selective-area growth (SAG) of doped GaN enables eliminating the lateral resistance and current crowding, especially if combined with material composition grading.[11]

In this work we analyze how the use of DDCT affects the device efficiency and discuss the associated changes in the device band diagram that enable the improvements. We also propose that realizing the linear composition grading all the way from the QW material composition to GaN can be used both to increase the effective thickness of the AR and to further facilitate the current transport in DDCT. Both of the latter benefits have been studied separately in Refs.,[11,12] but this paper combines both effects in the same device. Our results show that increasing the thickness of the AR with composition grading shifts the peak efficiency to higher current densities and decreases the efficiency droop. In the DHJ design, current crowding still causes an additional reduction of the device efficiency at large currents, but according to our results such an efficiency loss can be practically eliminated using DDCT and SAG. In addition, our results on single-side graded structures demonstrate how DDCT can be used to remove voltage losses due to electrons surpassing a polarization-induced potential barrier, as both electrons and holes enter the AR from the graded side in DDCT. In addition to the simulations, we perform SAG of a finger structure suitable for operation as an LHJ device.

Figure 1 shows the DHJ and lateral heterojunction (LHJ) structures simulated in this paper. All the structures have an n-type GaN bottom layer, a 2.5nm thick layer of homogeneous $In_{15}Ga_{85}N$, a linearly graded $In_{15}Ga_{85}N$/GaN layer and 150nm thick layer of p-GaN (and a similarly thick adjacent n-GaN layer in (b)). The 2.5nm thick InGaN layer and the bottommost nanometers of the graded layer together act as the AR, where the recombination predominantly takes place. To illustrate how current crowding depends on the device dimensions, two different 2-dimensional DHJ structures shown in Fig. 1(a) are studied: in the DHJ-100 and DHJ-250 structures, the separations between adjacent n-contacts are 100μm and 250μm, respectively. The LHJ structure of Fig. 1(b) has adjacent n- and p-type layers realized with selective-area growth on top of the graded layer, and both electrons and holes are transported to the AR from its top side by DDCT. The top n-GaN layer is 3μm wide and the top p-GaN layer is 10μm wide to account for the lower conductivity of p-GaN, and the separation between n-GaN and p-GaN is 1μm. To compare the 2-dimensional DHJ and LHJ devices with a purely 1-dimensional structure, Fig. 1(c) shows an ideal vertical LED (structure DHJ-0) with perfect transparent n- and p-type contacts on both sides. The resistive loss in the DHJ-0 structure does not contain any lateral

resistance, and its resistance is essentially caused by transport through the 150nm thick doped layers and the 100nm thick graded layer. Therefore it provides an idealized reference structure with no current crowding.

2. THEORY

Current transport is simulated in the LED structures of Fig. 1 using the drift-diffusion (DD) model (see, e.g. Refs.[13–16]), which solves self-consistently the device operation and, in particular, provides an adequate treatment of current crowding. The DD model is given by

$$\begin{aligned} \nabla \cdot (-\varepsilon \nabla \phi) &= e\,(p - n + N_d - N_a) - \nabla \cdot \mathbf{P_{tot}} \\ \nabla \cdot \mathbf{J}_n &= \nabla \cdot (-e\mu_n n \nabla \phi_n) = eR \\ \nabla \cdot \mathbf{J}_p &= \nabla \cdot (-e\mu_p p \nabla \phi_p) = -eR, \end{aligned} \tag{1}$$

where ε is the static permittivity, e is the elementary charge, μ_n, μ_p are the electron and hole mobilities, N_d, N_a are the ionized donor and acceptor doping densities, and $\mathbf{P}_{tot}$ is the total static polarization density consisting of spontaneous and piezoelectric polarization. The DD model relates the electrostatic potential ϕ and the quasi-Fermi levels $E_{Fn} = -e\nabla\phi_n$ and $E_{Fp} = -e\nabla\phi_p$ (ϕ_n and ϕ_p being the quasi-Fermi potentials) to the electron and hole densities n and p, electron and hole currents $\mathbf{J}_n$ and $\mathbf{J}_p$, and the recombination rate density throughout the device. In Eq. (1), N_d is further assumed to be equal to the total donor doping density, whereas N_a is calculated from the valence band quasi-Fermi level using the Fermi-Dirac distribution with an acceptor ionization energy of 170 meV, as in Ref.[9]

In Eq. (1), recombination rate R is calculated based on the electron and hole densities as detailed in Ref.[17] using the A, B and C coefficients for Shockley-Read-Hall (SRH), net radiative, and Auger recombination. Note that as the thin InGaN layer in Fig. 1 is graded from its other side and as the AR therefore is effectively much wider than the nominal 2.5nm, we do not separately account for any 2D carrier densities or recombination rates. Considerable uncertainty surrounds the calculation of Auger recombination in III-N devices (see, e.g., Ref.[18]). However, we note that as we mainly focus on electron and hole currents in the bulk layers and as the AR properties are similar between the structures under comparison, the conclusions of this paper should hold even if different Auger recombination models are used in the calculations. Internal quantum efficiency (IQE) is calculated from the simulations as R_{rad}/R_{tot}, where R_{rad} is the net radiative recombination rate and R_{tot} is the total net recombination rate. Wall-plug efficiency (WPE) is calculated as $P_{opt}/(UI)$, where P_{opt} is the optical output power calculated with a constant extraction efficiency of 0.9, and UI is the electrical input power.

The simulations are carried out using donor and acceptor densities of 5×10^{18} cm^{-3} and 1×10^{19} cm^{-3} in the n- and p-doped layers, respectively. The electron and hole mobilities in the doped layers are 230cm^2/(Vs) and 10cm^2/(Vs) based on our Hall measurements on previous samples. In unintentionally doped GaN, the electron and hole mobilities are 1000cm^2/(Vs) and 70cm^2/(Vs) based on Monte Carlo calculations reported in Ref.[19] The recombination parameters are set to $A = 10^7$ 1/s, $B = 5 \cdot 10^{-17}$ m^3/s and $C = 10^{-42}$ m^6/s in accordance with our previous work.[16] The polarization densities are scaled by 0.5 from the theoretical values reported in Ref.[20] to account phenomenologically for unidealities that are expected to partly compensate the polarization charges, such as defects and Indium fluctuations.[21,22]

3. RESULTS & DISCUSSION

Figure 2 shows the simulated current-voltage characteristics, where the current density is defined by dividing the total current with the full device area including contacts. The LHJ structure has a smaller voltage for a given current than the DHJ structures at all current densities. At small current densities this is due to a more favorable 2D band profile in the LHJ (to be discussed later) that decreases the voltage losses in the barrier layers. Of all the DHJ structures, the DHJ-0 structure shows much less saturation in its current-voltage curve at large currents than the other DHJ structures, since it does not contain any lateral current spreading. The current-voltage characteristics of the DHJ-100 and especially the DHJ-250 structure start to saturate already at current densities much below 100 A/cm^2 due to the resistive loss in the n-GaN layer and the corresponding current crowding. Quite remarkably, the LHJ structure shows almost as little saturation as the DHJ-0 structure at the current densities studied in Fig. 2, indicating very small lateral losses.

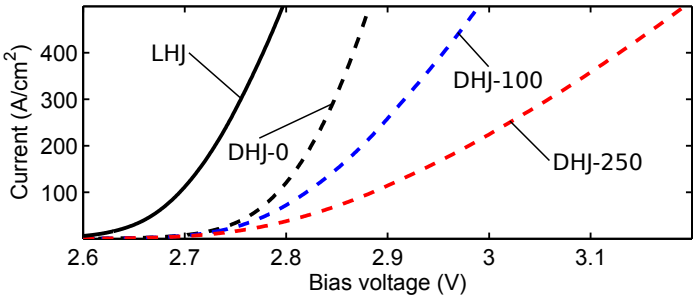

Figure 2. Current-voltage characteristics resulting from the simulations excluding contact resistances.

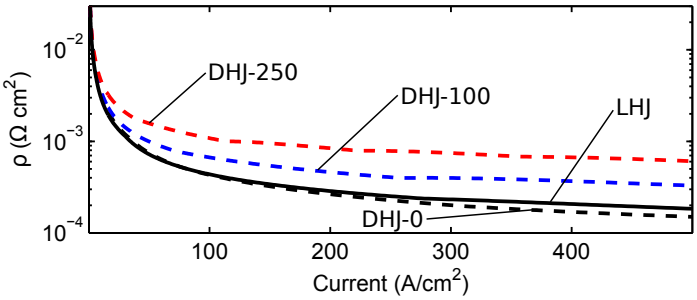

Figure 3. Differential resistance ρ of the structures defined as dU/dJ as a function of current density.

The resistive losses are easier to quantify by examining the differential resistance as a function of the current density. Figure 3 shows the differential resistance defined as $\rho = dU/dJ$ for all the structures from the simulations. As expected, the DHJ-0 structure shows the least differential resistance at large currents, as it does not contain any lateral current transport and as its resistive losses are therefore essentially caused by the 150nm thick doped layers and the 100nm thick graded layer. The DHJ-100 and DHJ-250 structures show significantly larger differential resistances than the DHJ-0 structure mostly due to the lateral resistive loss and the related current crowding in the n-GaN layer. In contrast, the LHJ structure has only slightly larger differential resistance than the ideal DHJ-0 structure, and its differential resistance is therefore significantly smaller than that of the DHJ-100 and DHJ-250 structures.

To illustrate the differences in the device operation in more detail, Fig. 4 shows the band diagrams of (a) the LHJ structure and (b) the DHJ-100 structure at a current density of roughly 250 A/cm^2. The band diagrams are plotted following the dashed arrows in Fig. 1, which roughly correspond to the center points of the ARs. The operating voltage is 2.75V in (a) and 2.9V in (b), reflecting that the LHJ requires a smaller operating voltage due to more favorable carrier injection and smaller current crowding. The more favorable carrier injection in the LHJ structure is illustrated in Fig. 4 using the symbols for electrons and holes: in the LHJ structure in (a), both electrons and holes enter the low-bandgap region responsible for light emission from the same side on the right. In the DHJ structure in Fig. 4(b), on the other hand, electrons enter the low-bandgap region from the left, where they have to surpass the polarization-induced potential barrier. In the structures simulated here, the large effective volume of the graded AR generates a fairly high recombination rate and consequently a large electron current density already at small bias voltages. Due to the small bias voltage, the potential barrier in Fig. 4(b) is not notably diminished by free-carrier screening even when a large electron current has to surpass it. This causes an electrical loss for electrons in the form of a quasi-Fermi loss as explained in more detail in Ref.,[16] and this loss also causes the ca. 0.1V difference in the low-bias operating voltages of the LHJ and DHJ devices seen in Fig. 2. Even if the quasi-Fermi loss can be expected to at least partly follow from incomplete treatment of carrier transport at the GaN/InGaN interface, such a loss may nonetheless be important at least in multi-quantum well devices, where electrons would need to transfer over multiple GaN barriers before reaching the uppermost QW with the highest hole concentration in the DHJ scheme.

To study the effects of current crowding on the device efficiency, Fig. 5(a) shows the internal quantum efficiency (IQE) for all the structures as a function of current density. All the structures show essentially similar

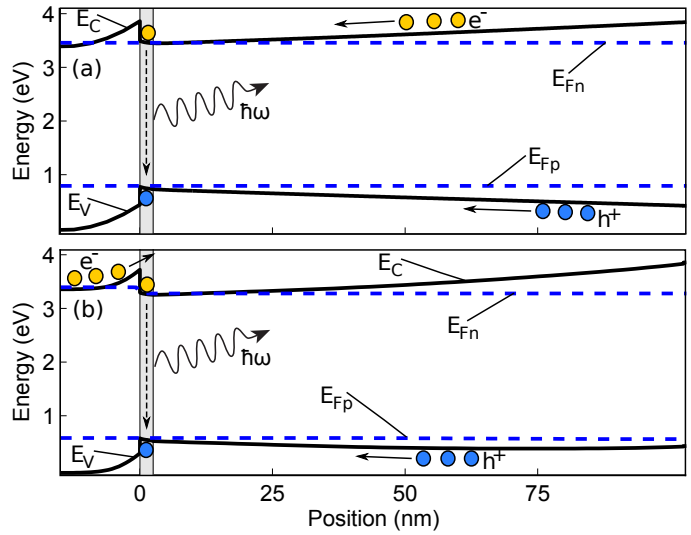

Figure 4. Band diagrams of (a) the LHJ structure and (b) the DHJ-100 structure at roughly 250 A/cm^2. The band diagrams are plotted following the dashed arrows marked in Fig. 1, and the zero position corresponds to the bottom interface of the InGaN AR. The bias voltages are (a) 2.75V and (b) 2.9V. The 2.5nm thick homogeneous InGaN layer is marked with a gray background, and the graded InGaN/GaN layer is on its right side.

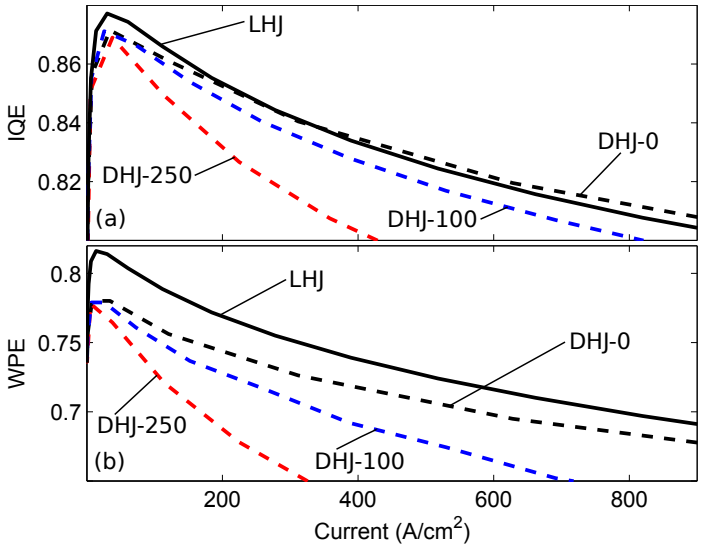

Figure 5. (a) Internal quantum efficiency and (b) wall-plug efficiency (excluding contact resistances) of the structures.

peak IQEs as expected, as all the devices have essentially similar active regions. Furthermore, especially the DHJ-0 structure has a very modest IQE droop due to the large effective AR thickness and the lack of any lateral current transport losses. On the other hand, both the DHJ-100 and the DHJ-250 structures show a more severe IQE droop than the DHJ-0 structure, and this difference is essentially caused by lateral carrier spreading, illustrating the additional effect of current crowding on the IQE droop. Especially the DHJ-250 structure has a large added IQE droop due to its wider p-contact region, but even the DHJ-100 structure exhibits a substantially more severe droop than the ideal DHJ-0 structure. The LHJ structure, on the other hand, differs only very little from the DHJ-0 structure within the current density range shown in the figure. This illustrates that it suffers much less from lateral current crowding than the 2-dimensional DHJ structures.

Since all the devices have essentially unity injection efficiency in the simulations, the IQE behaviour of the devices in Fig. 5(a) is also fully reproduced in their external quantum efficiencies, if the light extraction efficiencies

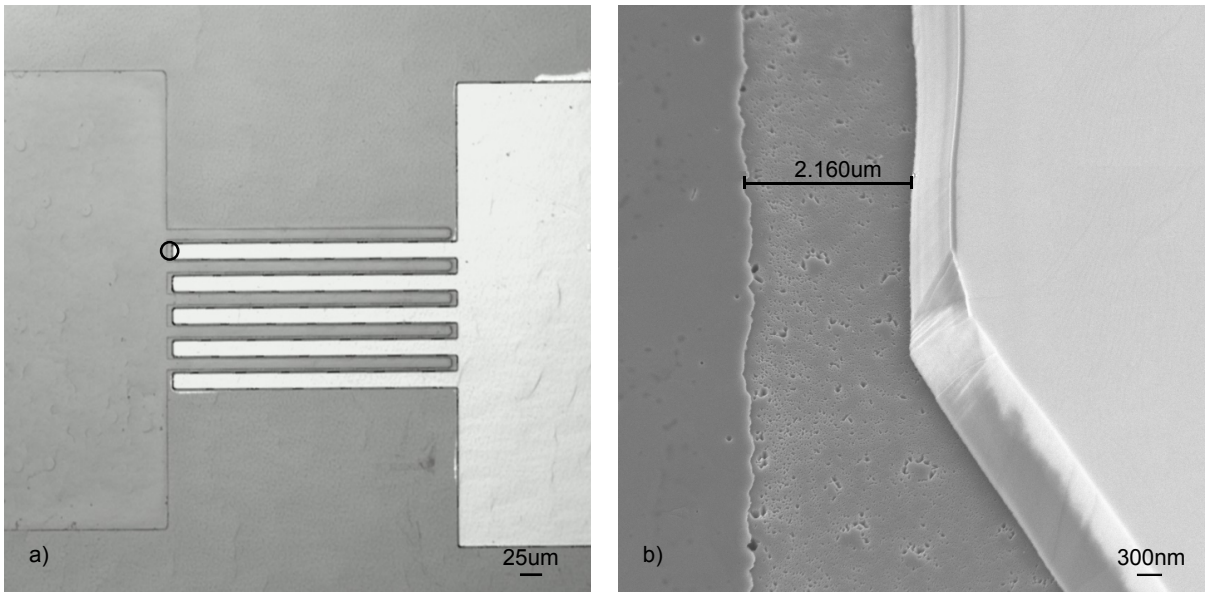

Figure 6. (a) Microscope image of the fabricated structure with separately grown n- (left) and p-GaN (right) regions. (b) SEM image of the area circled in (a) with the measured distance between the grown materials.

are similar. However, to illustrate the additional effect of the different bias voltages observed in Fig. 2, Fig. 5(b) shows the wall-plug efficiency (WPE) as a function of the current density for all the structures. As in the case of IQE, the DHJ-100/DHJ-250 structures show a stronger WPE droop than the ideal DHJ-0 structure. However, the difference between the DHJ-100/DHJ-250 and the DHJ-0 structure is larger in the case of WPE than in the case of IQE, since the DHJ-100/DHJ-250 structures require larger bias voltages than DHJ-0 at large current densities due to their lateral resistances. Most importantly, however, the LHJ structure shows superior WPE as compared to all the other structures. The larger peak WPE of the LHJ structure is caused by its roughly similar peak IQE together with a smaller voltage for a given current density as seen in Fig. 2. The smaller input voltage results in a smaller input power for a given current density in the LHJ structure. However, it can be seen in Fig. 5 that even if the peak WPEs were similar, the WPE droop from its peak value is less severe in LHJ than in the DHJ-100 structure, albeit still somewhat stronger than in the 1-dimensional ideal DHJ-0 structure. This illustrates the potential of the LHJ concept to boost the output power of LEDs at high currents.

LHJ devices can be realized e.g. by using SAG on a template wafer with the QW and the graded layer. The n- and p-type layers are then grown in separate epitaxial processes with a lithographically patterned growth mask. Example of an SAG-grown GaN-based LHJ structure is shown in Fig. 6. Fig. 6(a) shows a microscope image of a test structure with a separately grown n-GaN region (mesa and fingers on the left) and an opening in the growth mask made for the p-GaN region (mesa and fingers on the right). Fig. 6(b) shows an SEM image from the circled area in (a) for a structure where the SAG of both the n- and p-type GaN regions has been completed and the growth mask has been removed. In the figure the distance measured between the n- and p-GaN regions is approximately 2μm. The fabricated sample was grown using metallo-organic vapor phase epitaxy (MOVPE). First, templates consisting of a c-plane sapphire substrate, 5μm thick unintentionally doped intrinsic GaN (i-GaN) buffer layer, a standard 5 well InGaN/GaN MQW active region and 120nm i-GaN capping were grown. This template was then used as a substrate for n-GaN and p-GaN SAG processes. The SAG growth mask was fabricated by standard lithography techniques and an SiO_2 layer deposited by PECVD. The precursors for the growth were trimethyl gallium (TMG), trimethyl indium (TMI), and trimethyl aluminium (TMA).

4. CONCLUSIONS

We carried out full-device simulations of conventional LEDs and a comparable lateral heterojunction (LHJ) LED, where the carrier injection was realized using the diffusion-driven charge transport concept. Our results showed that using a single-side graded active region both facilitates the current transport in the LHJ device and leads to

a modest efficiency droop by increasing the effective thickness of the active region. More importantly, comparing the operation of the LHJ structure with conventional LEDs and an ideal vertical LED showed that the LHJ structure shows practically no added differential resistance or efficiency loss due to lateral current crowding. The LHJ structure could therefore provide a viable solution for realizing efficient high-power LEDs operating at current densities in excess of 100 A/cm^2 while allowing to separately engineer the material layers below the AR for optimal AR quality. Furthermore, the LHJ structure studied here showed an additional efficiency gain even over the ideal vertical LED thanks to injecting electrons and holes to the active region from the same side. As the top side of the active region did not have any significant potential barriers to either carriers, the LHJ structure operated with a smaller input voltage than any of the conventional structures. We expect this property to be even more interesting in multiple quantum well structures, where carriers typically need to surpass several potential barriers in conventional LEDs before being able to recombine and produce photons. One of the main challenges in selective-area growth of the LHJ devices is the fabrication of laterally located n- and p-layers with suitable geometry and spacing. Here we also demonstrated that it is possible to reach micrometer scale growth resolution with selective-area growth using standard fabrication techniques and growth masks combined with additional growth cycles. This should provide the means to fabrication of full device prototypes.

ACKNOWLEDGMENTS

Financial support from the Nokia Foundation, Finnish Cultural Foundation and Walter Ahlström Foundation, Academy of Finland and the European Research Council through the European Union's Horizon 2020 Research and Innovation Programme under Grant 638173 is gratefully acknowledged. The experimental part was undertaken at the Micronova Nanofabrication Centre of Aalto University.

REFERENCES

[1] S. Nakamura and M. R. Krames, Proc. IEEE **101**, 2211-2220 (2013).
[2] S. Y. Karpov, Proc. SPIE **9768**, 97680C (2016).
[3] H.-Y. Ryu and J.-I. Shim, Opt. Expr. **19**, 2886 (2011).
[4] C.-K. Li and Y.-R. Wu, IEEE T. Electr. Dev. **59**, 400 (2012).
[5] L. Wang, Z.-H. Zhang and N. Wang, IEEE J. Quant. Electr. **51**, 3200109 (2015).
[6] C. A. Hurni, A. David, M. J. Cich, R. I. Aldaz, B. Ellis, K. Huang, A. Tyagi, R. A. DeLille, M. D. Craven, F. M. Steranka and M. R. Krames, Appl. Phys. Lett. **106**, 031101 (2015).
[7] J. J. Wierer, D. A. Steigerwald, M. R. Krames, J. J. O'Shea, M. J. Ludowise, G. Christenson, Y.-C. Shen, C. Lowery, P. S. Martin, S. Subramanya, W. Götz, N. F. Gardner, R. S. Kern and S. A. Stockman, Appl. Phys. Lett. **78**, 3379 (2001).
[8] P. Kivisaari, J. Oksanen and J. Tulkki, Appl. Phys. Lett. **103**, 031103 (2013).
[9] L. Riuttanen, P. Kivisaari, O. Svensk, J. Oksanen and S. Suihkonen, IEEE T. Electr. Dev. **62**, 902 (2015).
[10] L. Riuttanen, P. Kivisaari, O. Svensk, J. Oksanen and S. Suihkonen, Appl. Phys. Lett. **107**, 051106 (2015).
[11] P. Kivisaari, I. Kim, S. Suihkonen and J. Oksanen, submitted for publication (2016).
[12] P. Kivisaari, J. Oksanen and J. Tulkki, Appl. Phys. Lett. **103**, 211118 (2013).
[13] K. A. Bulashevich, V. F. Mymrin, S. Karpov, Z. A. I. Zu and I. A. Zhmakin, J. Comput. Phys. **213**, 214 (2006).
[14] J. Piprek, F. Römer and B. Witzigmann, Appl. Phys. Lett. **106**, 101101 (2015).
[15] G. Verzellesi, D. Saguatti, M. Meneghini, F. Bertazzi, M. Goano, G. Meneghesso and E. Zanoni, J. Appl. Phys. **114**, 071101 (2013).
[16] P. Kivisaari, J. Oksanen and J. Tulkki, J. Appl. Phys. **111**, 103120 (2012).
[17] O. Heikkilä, J. Oksanen and J. Tulkki, J. Appl. Phys. **105**, 093119 (2009).
[18] J. Piprek, F. Römer and B. Witzigmann, Appl. Phys. Lett. **106**, 101101 (2015).
[19] E. Bellotti and F. Bertazzi, "Transport parameters for electrons and holes" in *Nitride Semiconductor Devices*, edited by J. Piprek (Wiley-VCH, Weinheim, 2007).
[20] V. Fiorentini, F. Bernardini and O. Ambacher, Appl. Phys. Lett. **80**, 1204 (2002).
[21] H. Zhang, E. J. Miller, E. T. Yu, C. Poblenz and J. S. Speck, Appl. Phys. Lett. **84**, 4644 (2004).
[22] T.-J. Yang, R. Shivaraman, J. S. Speck and Y.-R. Wu, J. Appl. Phys. **116**, 113104 (2014).